

**VRBA2024-00002**

## FRAME DESIGN OF INLINE SKATES MADE BY ADDITIVE TECHNOLOGY

E. Posmykova<sup>1</sup>, J. Hruban<sup>1</sup>, J. Mesicek<sup>1</sup>, R. Blaha<sup>1</sup>, Q.-P Ma<sup>1</sup>, J. Hajnys<sup>1</sup>, J. Petru<sup>1</sup>

<sup>1</sup>VSB -Technical University of Ostrava, Department of Machining Assembly and Engineering Metrology, Faculty of Mechanical Engineering, Ostrava, Czech Republic

\*Eliska Posmykova; e-mail: eliska.posmykova.st@vsb

### Abstract

The aim of the article was to investigate the possibility of topological optimization (TO) of the inline skate frame manufactured through the Powder Bed Fusion (PBF) method of AISi10Mg-0403, an Additive Manufacturing (AM) technique. The study's core objective was to leverage The Altair Inspire software to re-envision the initial CAD model, culminating in an organic and bionic frame design. Incorporating comprehensive load analysis, the research considered various load scenarios, including static mass, dynamic forces, and acceleration during cornering, to ascertain the frame's strength and stability. Topological optimization was excluded within a defined design space, preserving critical functional elements while enhancing performance. The first part of the article is devoted to defining the concepts and nature of AM metallic materials. The practical part follows, in which the design of the skate frame is specified with specific requirements and the procedure of individual steps needed to create its final CAD Model. The work concludes by describing the preparation of the designed optimized frame construction.

### Keywords:

Topology optimization, mechanical engineering design, frame, inline skates, Additive Manufacturing, Powder Bed Fusion

## 1 INTRODUCTION

The Powder Bed Fusion (PBF) is an Additive Manufacturing (AM) technology that joins powder material layer by layer creating a three-dimensional body, using an energy source, typically a laser beam or an electron beam [Marsalek, 2019]. This paper focuses on performing the topological optimization (TO) to design a frame for an Inline skate. We used the Altair Inspire software to optimize the initial CAD model of the frame and a new one with organic and bionic design was created.

The frame was manufactured with 3D printing technology with AISI 316L stainless steel by the PBF technology. With an organic shape this bionic design means use of more supports for the PBF method of AM and worse surface quality after their removal [Hajnys, 2019, Sedlak 2015].

For the design of the frame, the method of mounting the frame to the shoe, has a great importance. In this case, it is a screwed mounting bracket with a standard pitch of 195 mm. The shoe has threaded holes built in from the bottom. The frame will be a monolith piece, it will be made from one piece [Mikulikova, 2023].

## 2 MATERIALS AND METHODS

The frame is an integral part of inline skates and is important in transferring the forces [Sotola, 2021]. Variable forces are applied that are transferred from the shoe to the frame by friction between two surfaces. For their calculation, it has been considered the theoretical maximum load that the frame can bear when using it [Měsíček, 2022].

Topological optimization was excluded within a defined design space, preserving critical functional elements while enhancing performance. The static mass of the skater and the external dynamic forces have a major influence on its functional behavior [Kumar, 2022]. The frame design is designed to be lightweight. The top-down workflow of the the study is shown in Fig. 1.

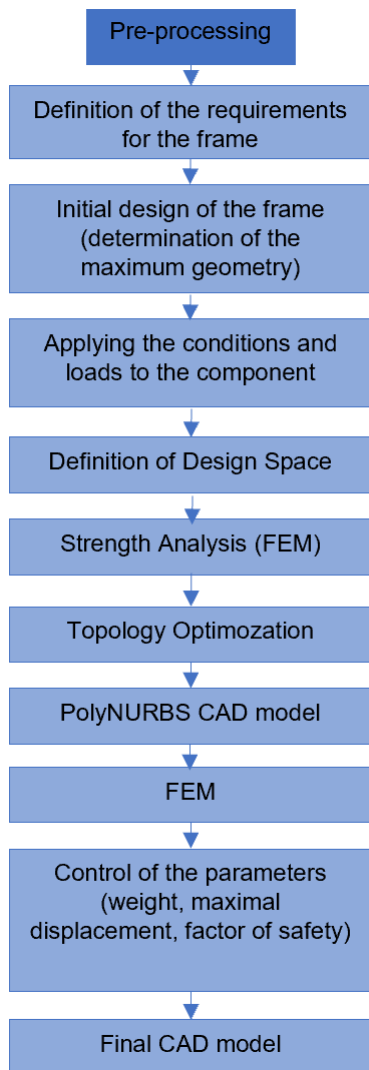


Fig. 1: The process of designing the In-line skate frame

The frame design was created in the largest possible dimensions. Holes for mounting skate wheels, space for wheels, and seating surfaces for inline skate boots have been preserved.

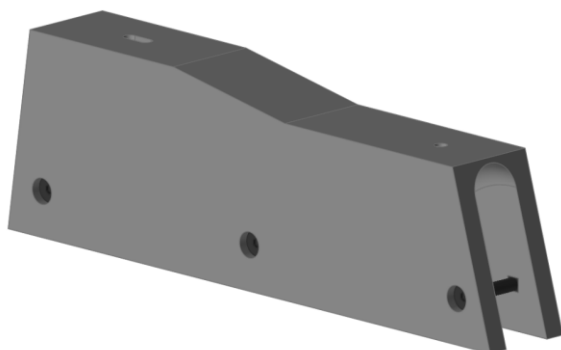


Fig. 2: The initial design of the In-line skate frame created with maximized dimensions.

### 3 RESULTS AND DISCUSSION

#### 3.1 Analytical solution

In this step, the analysis of load conditions and boundary conditions that determine the form of the skate frame design,

was carried out. After creating a model of the frame with the maximum possible geometry, consideration was made over a possible transfer of forces that arises when the skater puts on his skate and stands on it [Sotola, 2020a].

It is found that the resulting vertical load acts at three points marked as A, B, and C in Fig. 3. It also shows the load distribution and concentration pressure points, from which the force is transmitted first to the mounting elements between the frame and boot of inline skates and then to individual axles of the frame [Raičević, 2023].



Fig. 3: Scheme of load distribution of skater weight on the frame.

After considering how the forces are transferred from the skater through the frame to the individual wheels, in the next phase specific load conditions, which can occur when using inline skates, were contemplated [Cedzo, 2023].

In the following points, these individual load conditions are listed with the load cases:

##### 3.1.1. Standing in place on the front and then on the rear wheel

The mass of the 85 kg skater will exert a static load case on the front and then the back wheel of the skate. The Fig. 4 shows the load condition visually.

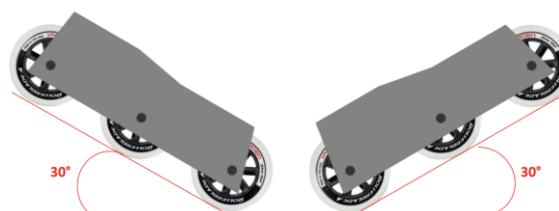


Fig. 4: Standing in place on the front and then on the rear wheel.

Calculation of the forces acting on the wheel axle at the first load condition:

$$F_1 = m \cdot g \quad [N] \quad (1.1)$$

$$F_1 = 85 \cdot 9.81$$

$$F_1 = 833.85 \cong 834 \text{ N}$$

The force F1 is the force of the load case and m is the mass of the skater applied to the inline skates.

### 3.1.2. Cornering with the inline skates

The scheme of cornering on inline skaters is shown in Fig. 5. In this load condition, all 6 wheels of the inline skates are in contact with the terrain. This is a dynamic load case. For calculating the load case it was necessary to know the acceleration of the acceleration of the skater's movement. The acceleration has value of  $1,168 \text{ m} \cdot \text{s}^{-2}$ .

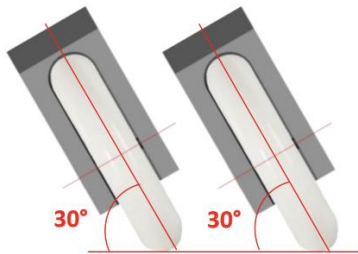


Fig. 5: The scheme of the inline skates when cornering.

The mass of the 85 kg skater will exert a force on the frame. The force on one wheel was calculated by dividing the force on the frame by the number of wheels:

$$F_g = \frac{m \cdot g}{6} \text{ N} = \frac{85 \cdot 9.81}{6} \text{ N} \cong 139 \text{ N}. \quad (1.2)$$

Then the force generated by the acceleration Fa was calculated:

$$F_a = \frac{m \cdot a}{6} \text{ N} = \frac{85 \cdot 1.168}{6} \text{ N} \cong 17 \text{ N}. \quad (1.3)$$

The friction force Ft was calculated, where  $\mu$  is the coefficient of friction ( $\mu=0.8$ ):

$$F_t = \frac{\mu \cdot m \cdot g}{6} \text{ N} = \frac{0.8 \cdot 85 \cdot 9.81}{6} \text{ N} \cong 111 \text{ N}. \quad (1.4)$$

The force vector F/ produced during the dynamic motion was determined:

$$F/ = |F_a - F_t| \text{ N} = |17 - 111| \text{ N} = 94 \text{ N}. \quad (1.5)$$

The resulting force F2 for this load case was calculated:

$$F_2 = \sqrt{F_g^2 - F/^2} \text{ N} = \sqrt{139^2 - 94^2} \text{ N} = 167.8 \text{ N}. \quad (1.6)$$

### 3.1.3 Starting and pushing off on the inline skates

This load condition represents the standard driving method. The pushing off is always performed with the back leg, which is tilted at an angle of  $60^\circ$  as seen in Fig. 6. The resulting force is evenly distributed among the axles of the individual wheels.

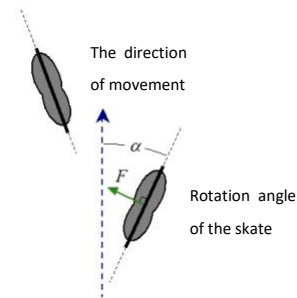


Fig. 6: The scheme of pushing off the inline skates

The resulting force F3 for the axle of the wheel of the third load condition was determined:

$$F_3 = \frac{m \cdot g}{3} \text{ N} = \frac{120 \cdot 9.81}{3} \text{ N} \cong 392 \text{ N}. \quad (1.7)$$

### 3.1.4 Impact from the height of one meter

The load condition considers the impact of the skate up to one meter. It can be a case of a jump of the skater or running off the curb, etc. This leads to the free fall, which causes the impact force acting on for axle of wheels as seen in Fig. 7. The load factor coefficient was selected to 3g.

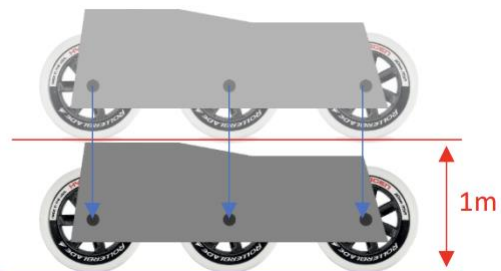


Fig. 7: The scheme of the impact from the height of one meter.

The resulting force F4 for the axle of the wheel of the fourth load condition was determined:

$$F_4 = \frac{m \cdot 3g}{3} \text{ N} = 85 \cdot 9.81 \text{ N} \cong 834 \text{ N}. \quad (1.8)$$

### 3.1.5 Braking

This is the last considered load condition in which the rear skate is rotated by 90°. On the skate begins to act moment and friction force. To determine the resulting the force had to be multiplied by the distance of the arm, which is the radius of the wheel (55 mm). The calculations of the forces are below:

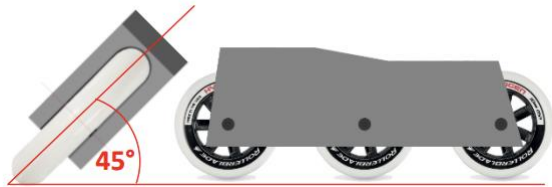


Fig. 8: The scheme of the braking.

$$F_a = (m \cdot a) N = (85 \cdot 1.168) N \cong 100 N, \quad (1.9)$$

$$F_t = (\mu \cdot m \cdot g) N = (0,8 \cdot 85 \cdot 9.81) N \cong 667 N, \quad (1.10)$$

$$F' = |F_a - F_t| N = |100 - 667| N = 567 N. \quad (1.11)$$

The resulting force F5 for the axle of the wheel of the fifth load condition was determined:

$$F_5 = [F' \cdot \sin(45^\circ)] N = [567 \cdot \sin(45^\circ)] N \cong 401 N. \quad (1.12)$$

The resulting moment M of applied force F5 on an arm with a length of 55 mm was calculated:

$$M = \frac{F \cdot R}{3} N \cdot m = \frac{401 \cdot 55}{3} N \cdot m \cong 7352 N \cdot m. \quad (1.13)$$

### 3.2 Topology optimization

The design space (the area where the simulation and shape modification in the form of the TO was performed) and the non-design space (preserved areas, functional parts of the frame) were specified [Hanzl, 2020].

The design space is the area that was used when calculating topological optimization. Therefore, it was necessary in the structural design of the skate frame to define geometric elements that had to be preserved due to subsequent assembly of the frame to the shoe of the skates, and wheels to the frame. Furthermore, symmetry condition was applied to the initial model of the frame according to the XY plane. This ensured the same force action on both sides. Therefore, it was not necessary to solve the tilt direction of the frame in the load cases [Rojas-Labanda & Stolpe, 2015].

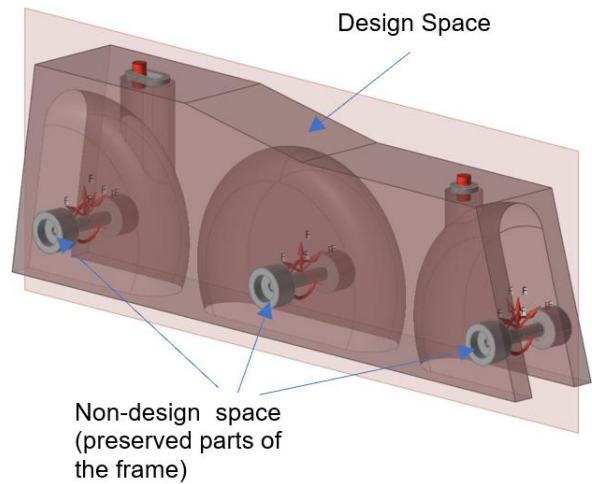


Fig. 9: Determination of Design and Non-design space.

### 3.2.1 FEM control analysis

Before performing the topological optimization itself, it was necessary to perform the strength analysis simulations to identify and check that the identified area has been designed properly [Gogolewski, 2023].

Table 1 lists the load input parameters for each load case. These load cases have been defined have been defined in the Altair Inspire software used for this TO of the frame.

Tab. 1: The input values of forces for individual load cases.

	Load case	Number of wheels in contact with the surface	The value
Standing in place on the front or on the rear wheel	$F_{1a}$ [N]	front wheel	834
	$F_{1b}$ [N]	rear wheel	834
Cornering	$F_2$ [N]	all six wheels	168
Pushing off	$F_3$ [N]	three wheels of one skate	392
Impact from the height of 1 m	$F_4$ [N]	three wheels of one skate	834
Braking	$M$ [N · m]	three wheels of one skate	7 352

The topology optimization was performed with the goal of maximizing the stiffness of the frame. The topological optimization parameters are shown in Tab. 2. The software generated the shape of the optimized part according to the load cases and the symmetry constraint [Sedlacek, 2023].

Tab. 2: The parameters of the TO.

The topological optimization parameters		
Mass Targets	Percentage of total design space volume	30%
Objective	Maximize Stiffness	
Thickness Constraints	Minimum	7 mm
	Maximum	14 mm

From the achieved result of topological optimization (which is visible in Fig. 10), it is clear, that most of the material has retained between the functional surfaces of the frame intended for mounting the shoe and axles of the individual wheels.



Fig. 10: The result of the TO in Altair Inspire software.

The PolyNURBS function was then used on the result of the frame optimization to create a smooth geometry. The outcome of PolyNURBS model's visual can be seen in Fig. 11.

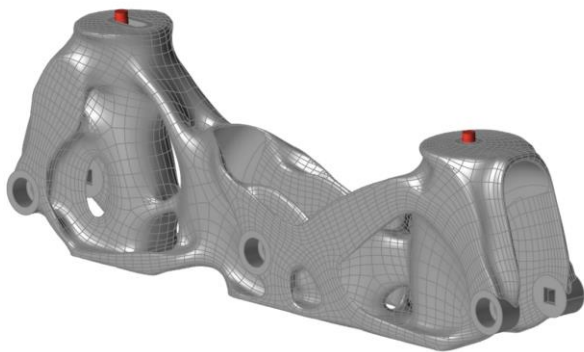


Fig. 11: The PolyNURBS geometry.

### 3.3 Fabrication with PBF

The data from the Altair Inspire software were transferred into .STL format for the transfer to other software and further customization options that can be done with the CAD model. The construction of the frame is quite large, therefore the orientation was limited by the dimension of the building chamber with the selection of a suitable orientation on the build platform. The Autodesk Netfabb software was used to determine the optimal orientation of the frame during the process of its manufacturing. The type of printer on which the prototype will be manufactured has been specified to Renishaw AM 500E [Poloprudský et al., 2022].

The software offered several options for the orientation of the prototype. The different options differ with these essential parameters: the support area, support volume, the built height, height of the centre of gravity. The optimal orientation has been selected based on comparison of these parameters.

In the Tab. 3 there are shown the parameters values for the different orientations. Orange values indicate the unsuitability of the parameter, on the other side, variants with predominantly green values are recommended for application for the part manufacturing. The variant of the orientation in the press chamber No. 1 with predominantly green values has been selected [Sotola, 2021].

Tab. 3: The parameters for individual variants of the frame orientation in the print chamber.

Variant	The support area [cm <sup>2</sup> ]	The support volume [cm <sup>3</sup> ]	The build height [mm]	The height of the centre of gravity [mm]
1	79.756	117.474	93.8	35.8
2	79.756	117.531	93.8	35.8
3	57.782	311.696	279.6	139.3
4	66.256	331.769	279.6	140.3
5	58.028	332.414	280.1	139.9
6	66.048	337.239	279.5	140.3

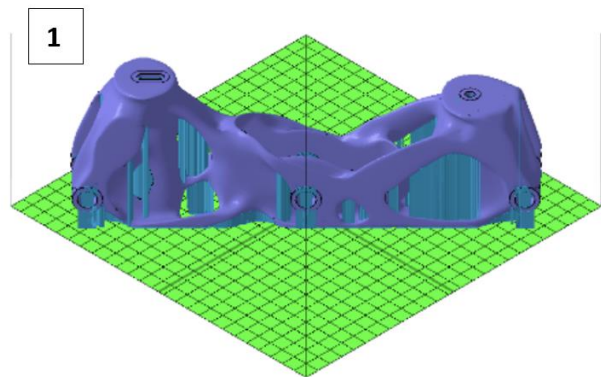


Fig. 12: The variant No. 1 of the orientation in the printing chamber.

The constructed frame has been rotated 45 ° around the Z-axis on the installation platform in a positive direction in the software. Supports were generated automatically, again in Altair Inspire. The part was also sliced and prepared for the build in this step. The data were transferred into the MTT format which is used by Renishaw printers [Gogolewski, 2021].

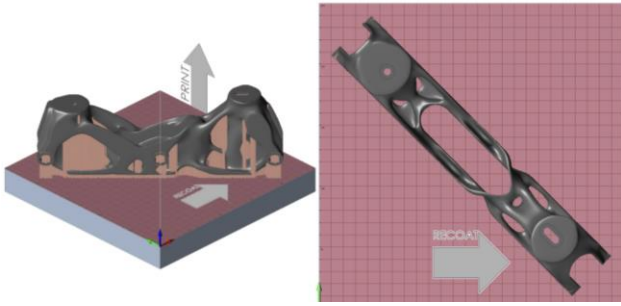


Fig. 13: The generated supports and preparing the build.

As mentioned before, the part was manufactured with the PBF technology, specifically the PBF method with the use of Renishaw AM 500E printer. The print parameters are shown in Tab. 4 [Sotola, 2020b].

Tab. 4: The parameters of the print

Parameters of the print	
Laser power [W]	1 x 500
Scanning speed [mm · s <sup>-1</sup> ]	650
Preheating temperature [°C]	170
Layer height [mm]	0.03
Number of layers [-]	3 295
Volume of material (powder) used [mm <sup>3</sup> ]	204 870
Printing time [h]	41

The material AISi10Mg-0403 was chosen to produce the frame of the inline skate due to its low density, high specific strength and its good response to surface finishing [Pirinu, 2023].

From the Tab. 5 we can see that the maximum displacement increased by 41% for the optimized frame, although the TO was performed with the condition of maximizing stiffness. The von Mises Stress increased by 18.3%. When comparing initial design space and the optimized frame [Pagac, 2021].

Tab. 5: The results of the FEM analysis of the initial design space and the optimized frame.

	The initial design space	The topologically optimized frame
Maximal displacement [mm]	0.569	0.803
Von Mises Stress [MPa]	334	395

The Fig. 14 shows an inline skate frame made using the PBF technology. The 3D printed frame is mounted to the shoe. A previous finishing operation was applied to the frame.



Fig. 14: The inline skate frame manufactured with the PBF technology.

## 4 CONCLUSION

In conclusion, this article delves into the innovative realm of topological optimization for designing an inline skate frame. In this process there have been taken the methodology of AM, specifically the PBF method (Fig. 14), to advantage. The journey through this study began with a comprehensive exploration of AM, progressing into the intricacies of manufacturing with metallic materials and analysis of the PBF method.

Critical to the success of the design was the integration of the frame with the shoe, emphasizing a screw-mounted bracket configuration that underscores the importance of proper force transmission and stability. The monolithic construction of the frame accentuates its robustness and ability to handle variable load cases that act on the frame during use.

Even if the goal of the article has been achieved, and it has been proven that it is possible to create a topologically optimized skate frame for the given conditions and load cases, there are possibilities for improving the design. Most of the mass of the optimized model is concentrated around the wheels of the inline skate. Which is not ideal for an inline skate frame in general. In further work on this design, it would be worth trying an optimization variant with a goal to minimize weight (instead of maximizing stiffness).

## 5 ACKNOWLEDGMENTS

This paper was supported in association with the project Innovative and additive manufacturing technology—new technological solutions for 3D printing of metals and composite materials, reg. No. CZ.02.1.01/0.0/0.0/17\_049/0008407 financed by Structural Funds of the European Union and project.

This article was funded by the European Union under the REFRESH – Research Excellence For Region Sustainability and High-tech Industries project number CZ.10.03.01/00/22\_003/0000048 via the Operational Programme Just Transition. Article has been also done in connection with project Students Grant Competition SP2023/088 „Specific Research of Modern Manufacturing Technologies for Sustainable Economy“ financed by the Ministry of Education, Youth and Sports and Faculty of Mechanical Engineering VŠB-TUO. The authors would like to thank Advanced Engineering s.r.o. for support in the topology optimization study.

## 6 REFERENCES

- [Cedzo, 2023] Cedzo, M., Joch, R., Timko, P., Holubjak, J., Czanova, T. & ˇSajgalik, M. (2023). Topology Optimization of Gripping Jaws of Industrial Robot. *Manufacturing Technology*, 23(1), 25–31. <https://doi.org/10.21062/mft.2023.009>
- [Gogolewski, 2021] Gogolewski, D., Kozior, T., Zmarzly, P. & Mathia, T. G. (2021). Morphology of Models Manufactured by SLM Technology and the Ti6Al4V Titanium Alloy Designed for Medical Applications. *Materials*, 14(21), 6249. <https://doi.org/10.3390/ma14216249>
- [Gogolewski, 2023] Gogolewski, D., Zmarzly, P. & Kozior, T. (2023). Multiscale Analysis of Functional Surfaces Produced by L-PBF Additive Technology and Titanium Powder Ti6Al4V. *Materials*, 16(8), 3167. <https://doi.org/10.3390/ma16083167>
- [Hajnys, 2019] Hajnys, J., Pagac, M., Kotera, O., Petru, J. & Scholz, S. (2019). INFLUENCE OF BASIC PROCESS PARAMETERS ON MECHANICAL AND INTERNAL PROPERTIES OF 316L STEEL IN SLM PROCESS FOR RENISHAW AM400. *MM Science Journal*, 2019(01), 2790–2794. [https://doi.org/10.17973/MMSJ.2019\\_03\\_2018127](https://doi.org/10.17973/MMSJ.2019_03_2018127)
- [Hanzl, 2020] Hanzl, P., Rulc, V., Purš, H., Zetek, M. & Zetkova, I. (2020). Lightweight design of milling cutter with modified stiffness. *Manufacturing Technology*, 20(4), 442–447. <https://doi.org/10.21062/mft.2020.099>
- [Kumar, 2022] Kumar, N., Singh, R. K., Srivastava, A. K., Nag, A., Petru, J. & Hloch, S. (2022). Surface Modification and Parametric Optimization of Tensile Strength of Al6082/SiC/Waste Material Surface Composite Produced by Friction Stir Processing. *Coatings*, 12(12), 1909. <https://doi.org/10.3390/coatings12121909>
- [Marsalek, 2019] Marsalek, P., Grygar, A., Karasek, T. & Brzobohaty, T. (2019). Virtual prototyping of 3D printed cranial orthoses by finite element analysis. *320010*. <https://doi.org/10.1063/1.5114332>
- [Mesicek, 2022] Mesicek, J., Cegan, T., Ma, Q.-P., Halama, R., Skotnicova, K., Hajnys, J., Jurica, J., Krpec, P. & Pagac, M. (2022). Effect of artificial aging on the strength, hardness, and residual stress of SLM AlSi10Mg parts prepared from the recycled powder. *Materials Science and Engineering: A*, 855, 143900. <https://doi.org/10.1016/j.msea.2022.143900>
- [Mikulikova, 2023] Mikulikova, A., Mesicek, J., Karger, J., Hajnys, J., Ma, Q.-P., Sliva, A., Smiraus, J., Srnicek, D., Cienciala, S. & Pagac, M. (2023). Topology Optimization of the Clutch Lever Manufactured by Additive Manufacturing. *Materials*, 16(9), 3510. <https://doi.org/10.3390/ma16093510>
- [Pagac, 2021] Pagac, M., Hajnys, J., Halama, R., Aldabash, T., Mesicek, J., Jancar, L. & Jansa, J. (2021). Prediction of Model Distortion by FEM in 3D Printing via the Selective Laser Melting of Stainless Steel AISI 316L. *Applied Sciences*, 11(4), 1656. <https://doi.org/10.3390/app11041656>
- [Pirinu, 2023] Pirinu, A., Primo, T., Del Prete, A., Panella, F. W. & De Pascalis, F. (2023). Mechanical behaviour of AlSi10Mg lattice structures manufactured by the Selective Laser Melting (PBF). *The International Journal of Advanced Manufacturing Technology*, 124(5–6), 1651–1680. <https://doi.org/10.1007/s00170-022-10390-1>
- [Poloprudsky, 2022] Poloprudsky, J., Nag, A., Kruml, T. & Hloch, S. (2022). Effects of liquid droplet volume and impact frequency on the integrity of Al alloy AW2014 exposed to subsonic speeds of pulsating water jets. *Wear*, 488–489, 204136. <https://doi.org/10.1016/j.wear.2021.204136>
- [Raicevic, 2023] Raicevic, N., Grbovic, A., Kastratovic, G., Vidanovic, N. & Sedmak, A. (2023). Fatigue life prediction of topologically optimized torque link adjusted for additive manufacturing. *International Journal of Fatigue*, 176, 107907. <https://doi.org/10.1016/j.ijfatigue.2023.107907>
- [Rojas-Labanda, 2015] Rojas-Labanda, S. & Stolpe, M. (2015). Benchmarking optimization solvers for structural topology optimization. *Structural and Multidisciplinary Optimization*, 52(3), 527–547. <https://doi.org/10.1007/s00158-015-1250-z>
- [Sedlacek, 2023] Sedlacek, F., Kalina, T. & Stepanek, M. (2023). Optimization of Components with Topology Optimization for Direct Additive Manufacturing by DLMS. *Materials*, 16(15), 5422. <https://doi.org/10.3390/ma16155422>
- [Sedlak 2015] Sedlak, J.; Sekerka, V.; Kouril, K.; Zemcik, O.; Chladil, J.; Rozkosny, L. Production of Prototype Parts Using Direct Metal Laser Sintering Technology. *Acta Polytechnica*, 55(4). <https://doi.org/10.14311/AP.2015.55.0260>
- [Sotola, 2021] Sotola, M., Marsalek, P., Rybansky, D., Fusek, M. & Gabriel, D. (2021). Sensitivity Analysis of Key Formulations of Topology Optimization on an Example of Cantilever Bending Beam. *Symmetry*, 13(4), 712. <https://doi.org/10.3390/sym13040712>
- [Sotola, 2020a] Sotola, M., Stareczek, D., Rybansky, D., Prokop, J. & Marsalek, P. (2020). New Design Procedure of Transtibial ProsthesisBed Stump Using Topological Optimization Method. *Symmetry*, 12(11), 1837. <https://doi.org/10.3390/sym12111837>
- [Sotola, 2020b] Sotola, M., Stareczek, D., Rybansky, D., Prokop, J. & Marsalek, P. (2020). New Design Procedure of Transtibial ProsthesisBed Stump Using Topological Optimization Method. *Symmetry*, 12(11), 1837. <https://doi.org/10.3390/sym12111837>